AGU PUBLICATIONS

Journal of Advances in Modeling Earth Systems

RESEARCH ARTICLE

10.1002/2016MS000668

The heated condensation framework as a convective trigger in the NCEP Climate Forecast System version 2

Rodrigo J. Bombardi[1], Ahmed B. Tawfik[2], Julia V. Manganello[1], Lawrence Marx[1], Chul-Su Shin[1], Subhadeep Halder[1], Edwin K. Schneider[1], Paul A. Dirmeyer[1], and James L. Kinter III[1]

[1]Center for Ocean-Land-Atmosphere Studies, George Mason University, Fairfax, Virginia, USA, [2]National Center for Atmospheric Research, Boulder, Colorado, USA

Key Points:
- Implementation of a New Convective Trigger Function into the parameterizations of convection in the CFSv2
- The new trigger function shows improvements in the representation of the intensity of tropical cyclones and rainy season
- The new trigger holds promise for future operational prediction systems

Correspondence to:
R. J. Bombardi,
rbombard@gmu.edu

Citation:
Bombardi, R. J., A. B. Tawfik, J. V. Manganello, L. Marx, C.-S. Shin, S. Halder, E. K. Schneider, P. A. Dirmeyer, and J. L. Kinter III (2016), The heated condensation framework as a convective trigger in the NCEP Climate Forecast System version 2, *J. Adv. Model. Earth Syst.*, *8*, 1310–1329, doi:10.1002/2016MS000668.

Received 7 MAR 2016
Accepted 23 JUL 2016
Accepted article online 2 AUG 2016
Published online 23 AUG 2016

Abstract An updated version of the Heated Condensation Framework (HCF) is implemented as a convective triggering criterion into the National Centers for Environmental Prediction (NCEP) Climate Forecast System version 2 (CFSv2). The new trigger replaces the original criteria in both the deep (Simplified Arakawa-Schubert – SAS) and shallow (SAS based) convective schemes. The performance of the original and new triggering criteria is first compared against radiosonde observations. Then, a series of hindcasts are performed to evaluate the influence of the triggering criterion in the CFSv2 representation of summer precipitation, the diurnal cycle of precipitation, and hurricanes that made landfall. The observational analysis shows that the HCF trigger better captures the frequency of convection, where the original SAS trigger initiates convection too often. When implemented in CFSv2, the HCF trigger improves the seasonal forecast of the Indian summer monsoon rainfall, including the representation of the onset dates of the rainy season over India. On the other hand, the HCF trigger increases error in the seasonal forecast of precipitation over the eastern United States. The HCF trigger also improves the representation of the intensity of hurricanes. Moreover, the simulation of hurricanes provides insights on the mechanism whereby the HCF trigger impacts the representation of convection.

1. Introduction

Recent advancements in high performance computing represent an exciting opportunity for global climate model development, pushing the limits of representing clouds and convection in a global atmospheric model [*Chen and Lin*, 2011; *Dirmeyer et al*., 2012; *Manganello et al*., 2012; *Murakami et al*., 2012; *Bacmeister et al*., 2014; *Wehner et al*., 2014]. As a consequence, atmospheric moist convection can now be represented in sophisticated schemes such as global cloud-resolving models and super parameterization schemes [*Grabowski*, 2001; *Khairoutdinov and Randall*, 2001; *Randall et al*., 2003; *Tomita and Satoh*, 2004; *Satoh et al*., 2008, 2014; *Stan et al*., 2010]. However, most schemes used to represent atmospheric moist convection in climate models still require the representation of processes that control the initiation of convection. Such processes are commonly known as convective trigger functions, which specify a criterion or a set of criteria that have to be satisfied in order for parameterized convection to initiate [e.g., *Chao* 2013]. Hereby we will refer to the convective trigger function as a "trigger criterion."

The trigger criteria in convective parameterization schemes are important for the correct representation of the timing of the diurnal cycle of convection and precipitation in atmospheric models [*Xie*, 2004; *Lee et al*., 2007a, 2008; *Silva and de Freitas*, 2015]. It is worth mentioning that the trigger criterion is just a simple representation of a suite of real physical processes. *Lee et al*. [2008] performed a comprehensive analysis of the convective triggering criteria in the Simplified Arakawa-Schubert deep parameterization scheme in the NCEP Global Forecasting System (GFS) atmospheric model. They found that the first trigger criterion in the convective parameterization scheme (related to a pressure difference between the convection starting level and the convective cloud base) plays a key role in the representation of the diurnal cycle of precipitation over the Great Plains in the United States. *Xie* [2004] introduced a dynamic constraint in the convective trigger criterion of the Community Atmosphere Model version 2 (CAM2) and verified that it improved not only the representation of the diurnal cycle of convection but also several other important fields including surface temperature and tropical high clouds on weather and subseasonal timescales.

Although the convective trigger criteria do not directly influence the nature or the intensity of convection, changes in the timing of convection modifies the accumulation of convective available potential energy (CAPE) over time. Therefore, the triggering criteria indirectly affect the environment that is used by the convective scheme, impacting the representation of atmospheric phenomena on a wide range of scales. *Ma and Tan* [2009] modified the convective parameterization scheme in the Mesoscale Model version 5 (MM5) by including the effect of moisture advection in the convective trigger criterion. They show that the distribution and the intensity of convective precipitation were significantly improved with the new algorithm. They also verified that the new algorithm improved tropical cyclone track simulation by about 10%. *Zadra et al*. [2014] verified that, by adjusting a parameter called "trigger velocity" in the trigger criterion of the Canadian Global Deterministic Prediction System (GDPS), they were able to reduce the false alarm rate of tropical cyclone forecasts, although the new configuration resulted in little difference in the tropical cyclone track error.

On intraseasonal timescales, *Wang and Schlesinger* [1999] studied the influence of convective parameterization in the representation of the Madden-Julian Oscillation (MJO) simulated by the University of Illinois at Urbana–Champaign (UIUC) atmospheric general circulation model. The authors found that the representation of the amplitude of the MJO was improved by including a relative humidity threshold criterion in the convective parameterizations. The inclusion of a relative humidity threshold in the parameterization scheme of the National Center for Atmospheric Research (NCAR) Community Climate Model version 3 (CCM3) improved the variability of the MJO in precipitation data [*Zhang and Mu*, 2005]. *Lin et al*. [2008] also verified that a moisture convective trigger improves the variance and the phase speed of coupled equatorial waves in the Seoul National University (SNU) atmospheric general circulation model.

In a recent paper, *Bombardi et al*. [2015, hereinafter B015] modified the convective triggering criterion in the deep convection scheme of the National Centers for Environmental Prediction (NCEP) atmosphere-ocean global coupled model (AOGCM) used for seasonal prediction, the Climate Forecast System version 2 (CFSv2) [*Saha et al*., 2014]. An additional criterion called the Heated Condensation Framework (HCF) [*Tawfik and Dirmeyer*, 2014] was added to the original trigger criterion in the Simplified Arakawa-Schubert convective scheme. This modification resulted in improvements in the CFSv2 representation of the Indian summer monsoon rainfall.

In this paper we present a follow-up to B015 using an updated version of the convective trigger criterion in SAS. Our hypothesis is that the CFSv2 precipitation biases can be reduced by improving the representation of convection through the improvement of the convective trigger criterion. It is worth mentioning that the initiation of convection refers only to the starting of a convective event and it is different from the continuation of convection [*Chao*, 2013].

This study is part of the National Monsoon Mission project supported by the Ministry of Earth Sciences, Government of India. The project has the objective of improving seasonal forecasts of the Indian Monsoon. A description of the CFSv2, the methods, and the main differences between this study and B015 are given in section 2. Section 3 describes the application of the original and new triggering algorithms to sounding data. The impact of the HCF trigger on seasonal simulations is investigated in section 4. Section 5 describes the impact of the new triggering criterion on the diurnal cycle of precipitation. The effect of the HCF trigger in the representation of hurricanes is investigated in section 6. Summary and conclusions are presented in section 7.

2. Model, Methods, and Previous Results

2.1. CFSv2 Model Description

The CFSv2 AOGCM atmospheric component is the NCEP Global Forecast System (GFS) model. We used spectral discretization at T126 resolution (about 100 km grid spacing) and 64 levels in the vertical. The oceanic component is the Modular Ocean Model version 4 (MOM4) [*Griffies et al*., 2004], with 1/2° horizontal resolution, increasing to 1/4° meridional resolution in the deep tropics, and 40 vertical levels. The sea ice component is a modified version of the Geophysical Fluid Dynamics Laboratory (GFDL) Sea Ice Simulator (described in *Saha et al*. [2010]) and the land surface model is Noah [*Ek et al*., 2003] version 2.7.1.

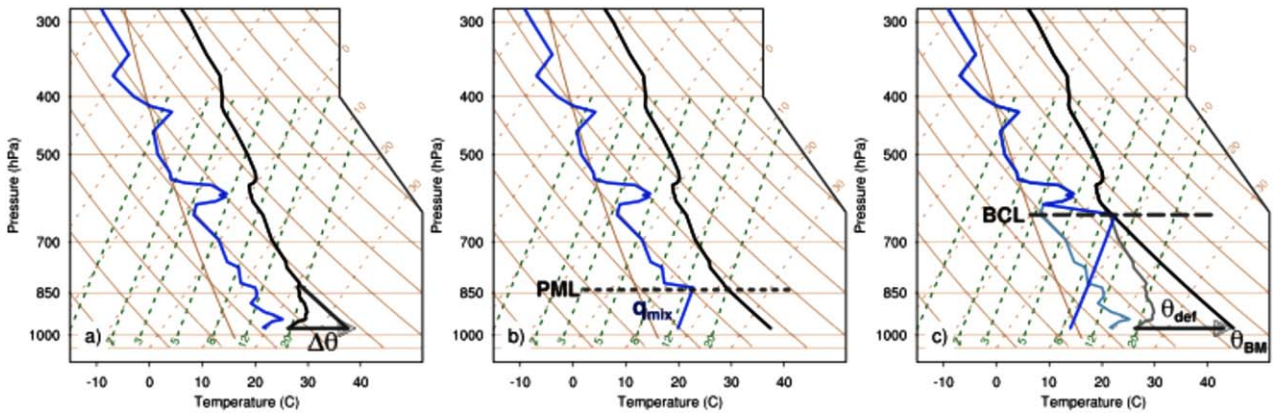

Figure 1. Thermodynamic profiles (e.g., skewT-logP diagrams) of temperature (black) and dew point temperature (blue) illustrating the steps for calculating the buoyant condensation level (BCL), buoyant mixing temperature (θ BM), and mixed layer specific humidity (q_{mix}). Dashed green lines represent constant mixing ratio lines, dashed tan lines represent isotherms and solid tan lines are dry adiabats. (a) Describes the first step where θ 2 m is perturbed by some increment, $\Delta\theta$. (b) Identifies the height, the potential mixed level (PML), where the perturbed surface parcel (θ 2m + $\Delta\theta$) is neutrally buoyant and the humidity profile is mixed from the PML to the surface. (c) θ2 m is perturbed until saturation occurs at the PML and the level is identified as the BCL. θdef is the total potential temperature increment necessary to reach θ BM from the initial θ 2m. Faint blue and grey lines in c) refer to the unperturbed profile shown in Figure 1a as a reference. Figure replicated from *Tawfik and Dirmeyer* [2014].

The atmospheric component of CFSv2 uses the Simplified Arakawa-Schubert (SAS) convective parameterization scheme, which is a mass-flux column model. There are two SAS routines currently in use in the CFSv2, informally known as "Old SAS" [*Pan and Wu*, 1995; *Hong and Pan*, 1998] and "New SAS" [*Han and Pan*, 2011]. *Han and Pan* [2011] describe an updated physics package for the CFSv2 including the revised version of SAS (New SAS), along with a SAS-based parameterization of shallow cumulus, and a revised scheme for the PBL. They show that the new physics package improves the model forecast skill, decreases vector wind forecast error, and improves hurricane tracks and atmospheric heating. However, the new physics package also increased the surface temperature bias and negative wind speed bias throughout the atmosphere. *Ganai et al*. [2015] evaluated the performance of several combinations of shallow and deep convection in representing the Indian Summer Monsoon using the CFSv2. They verified that the best configuration for representing the monsoon is the use of the New SAS deep convection scheme without using the SAS-based shallow cumulus. We reached the same conclusion in a series of sensitivity tests (not shown). However, for the purposes of model development, we made the conscious decision of using the most physically appropriate routines instead of using the operational configuration of the CFSv2. Therefore, in this study we use the New SAS and the SAS-based shallow cumulus schemes.

The native triggering criteria in both New SAS and SAS-based shallow cumulus is organized as follows: First, the starting point of convection is defined as the vertical level with the maximum moist static energy. Next, the cloud base is defined as the level of free convection (LFC) derived from the atmospheric stability profile above the level of maximum moist static energy. If the pressure difference between these two levels is between 120 and 180 hPa, convection is allowed to occur [*Han and Pan*, 2011; *Suhas and Zhang*, 2014]. This initial triggering criterion provides a necessary but not sufficient condition for shallow or deep convection to occur. For instance, the SAS-based shallow cumulus trigger criteria depends on other conditions such as the boundary layer height and convection inhibition due to the presence of a dry layers below the cloud base. Likewise, the New SAS trigger criteria also depends on many other factors such as entrainment, detrainment, and cloud work function also play a role in the development of convection. Convection is triggered only if all these criteria are met. Nonetheless, the pressure difference trigger is the first criterion in a series of trigger criteria, the other criteria are not even considered if the initial criteria are not met. A detailed description of all the criteria in the convective trigger criteria in SAS can be found in *Lee et al*. [2008].

2.2. New HCF Convective Triggering Criterion

The HCF was developed by *Tawfik and Dirmeyer* [2014] and further elaborated upon in *Tawfik et al*. [2015a,b]. The HCF was designed to represent the atmospheric background state with respect to convection using profiles of temperature and specific humidity. The HCF contains a diagnostic variable analogous to convective inhibition (CIN) but does not require the selection of an air parcel nor does it require the

Table 1. Configuration of Experiments

Exp. Name	Type	# of Years/ Events	# of Members	Horizontal Resolution	Temporal Resolution	Trigger Criteria
CTRL	Seasonal (7 months)	13	4	T126 (∼1.0°)	Daily	Original (pressure difference)
	Diurnal Cycle (∼2 weeks)	13	4	T126 (∼1.0°)	3 hourly	
	Hurricanes (30 days)	24	7	T382 (∼0.31°)	6 hourly	
HCFv2	Seasonal (7 months)	13	4	T126 (∼1.0°)	Daily	HCF
	Diurnal Cycle (∼2 weeks)	13	4	T126 (∼1.0°)	3 hourly	
	Hurricanes (30 days)	24	7	T382 (∼0.31°)	6 hourly	

existence of a level of free convection. Instead the HCF returns a variable referred to as the potential temperature deficit, θ_{def}, representing the heating needed to achieve saturation at the top of a well-mixed boundary layer.

θ_{def} is calculated by incrementally increasing the potential temperature, mimicking surface heating (see Figure 1). This pseudo-heating results in a hypothetical planetary boundary layer (PBL) whose top is located at the level at which the new lowest level potential temperature intersects the environmental lapse rate. The specific humidity profile is then mixed downward from the new hypothetical PBL height to the surface, once again to imitate growth of a well-mixed PBL. The lowest level potential temperature is incremented until saturation occurs at the top of the hypothetical PBL. This new level is referred to as the buoyant condensation level (BCL) and the amount of surface heating required to reach the BCL is $C_p\,\theta_{def}$, where C_p is the specific heat of dry air. θ_{def} and BCL height change only when temperature and humidity profiles evolve. Note that this construct is simply a diagnostic to discover the amount of surface heating required to achieve saturation accounting for moisture and temperature characteristics of a given profile. In this regard convection is triggered when θ_{def} decreases to zero, thus the analogy with CIN and applicability as a convective triggering criterion without assumptions about parcel selection or parcel mixing. It should be noted that the HCF is not a traditional CIN trigger, as it does not rely on parcel theory but rather on a well-mixed boundary layer diagnostic.

Rather than the diagnostic description of incremental surface heating described above, programmatically it is more efficient to calculate the mixed specific humidity q_{mix} and saturation specific humidity, q^*, for all explicit levels at each time step and then discover the level at which q^* minus q_{mix} is zero. The mixed specific humidity vertical profile is calculated by equation (1):

$$q_{mix}(z_i) = \frac{\sum_{k=k_{sfc}}^{i} [q_k \cdot \Delta p_k]}{\sum_{k=k_{sfc}}^{i} [\Delta p_k]} \tag{1}$$

where $q_{mix,}(z_i)$ is the mixed specific humidity at a model level z, q is the layer average specific humidity, and Δp is the pressure difference between the top and bottom model level interfaces. The index i refers to the level of interest, the index k refers to the layer average between two consecutive model layers, and k_{sfc} refers to the surface level. The potential temperature corresponding to the level where q^* minus q_{mix} is zero (i.e., the saturation level) is referred to as the buoyant mixing potential temperature, θ_{BM}.

θ_{def} is defined by subtracting the lowest model level potential temperature (or 2 m potential temperature, θ_{2m}) from θ_{BM} (equation (2)). In the CFSv2 we use 2 m virtual potential temperature $\theta_{v,2m}$ instead of θ_{2m} to appropriately respond to buoyancy-driven motions over the ocean and wet land areas (the same trigger is used over land and ocean).

$$\theta_{def} = \theta_{BM} - \theta_{v,2m} \tag{2}$$

and convection is triggered when $\theta_{def} = 0$.

θ_{def} has been shown to accurately capture convective triggering and the atmospheric background state with respect to convection over maritime land-sea breeze initiated convection [*Tawfik and Dirmeyer*, 2014], as well as responding to low-level jet and mesoscale convection systems over the United States Central Plains [*Tawfik and Dirmeyer*, 2014; *Tawfik et al*., 2015a]. Therefore, in order to initiate convection the HCF trigger requires the availability of large-scale convective instability allied with sufficient local surface heating. The HCF code can be accessed at https://github.com/abtawfik/coupling-metrics/blob/master/heated_condensation/static/hcfcalc.f90.

2.3. Experiments

We performed three suites of numerical experiments with CFSv2 (Table 1). Each suite was carried out in sets of control (CTRL) and modified trigger (HCFv2) experiments, where the HCF trigger was included in both deep and shallow cumulus parameterizations.

Since the motivation of our project is to improve the prediction of the Indian monsoon, the first set of simulations consists of seasonal hindcasts. Four ensemble members have been generated for each set of seasonal experiments for each year from 1998 to 2010, totaling 104 seasonal members. These hindcasts were initialized at 0000UTC in the first 4 days of April (1 through 4). Seasonal runs were integrated for 7 months and data were saved with daily temporal resolution. Similar to the seasonal runs, another suite of short simulations with higher temporal resolution (3 hourly) were carried out with the purpose to evaluate the impact of the HCF trigger on the diurnal cycle of precipitation. The diurnal cycle runs were initialized in the peak of the summer Indian monsoon in mid-July (14 through 17).

Since an important aspect of model physics for operational centers is the code's ability to represent tropical cyclones (TC), we also performed a third set of experiments focusing on hurricane events that made landfall in the Americas (Table 1). We selected long lasting major hurricanes that made landfall in the United States and a few other interesting cases such as hurricane Catarina [*Pezza*, 2005] that made landfall in Brazil (Table 2). Seven ensemble members were generated for each hurricane event and initialized at 1 day intervals, totaling 336 members. The initialization dates were the landfall date and the previous six dates prior to the event's landfall.

The initial conditions for all simulations were obtained from the NCEP Climate Forecast System Reanalysis (CFSR) [*Saha et al*. 2010]. The simulation outputs are compared to the Optimum Interpolation Sea Surface Temperature (OISST) [*Reynolds et al*., 2007], to the TRMM precipitation analysis [*Huffman et al*., 2007], and in the case of TC tracks to CFSR and to the International Best Track Archive for Climate Stewardship (IBTrACS) [*Knapp et al*., 2010].

2.4. Main Differences Between B015 and the Current Study

The main differences between this study and B015 are related to refinements of the convective schemes and the trigger criterion. B015 used the operational version of the CFSv2, which uses the Old SAS deep convection scheme and a turbulent diffusion shallow cumulus scheme. The introduction of the HCF trigger in B015 was done only in the deep convection scheme (Old SAS). In addition, the HCF trigger was included as an additional criterion, maintaining both the original Old SAS trigger criterion and the HCF criterion in the deep convection scheme. We also kept all the remaining trigger criteria in Old SAS unchanged.

Table 2. Hurricane Events

Hurricane Name	Year	Hurricane Name	Year
Arthur	2014	Isabel	2003
Sandy	2012	Floyd	1999
Irene	2011	Georges	1998
Ike	2008	Bonnie	1998
Gustav	2008	Fran	1996
Dean	2007	Emily	1993
Wilma	2005	Andrew	1992
Katrina	2005	Bob	1991
Emily	2005	Hugo	1989
Ivan	2004	Gilbert	1988
Frances	2004	Charley	1986
Catarina	2004	Gloria	1985

In this study, our control experiment (CTRL) uses the revised convection schemes, the New SAS deep convection scheme and a SAS-based shallow cumulus scheme. In our test experiment (HCFv2) the trigger criterion based on the pressure difference was completely replaced by the HCF trigger (it is not an additional criterion) in both deep and shallow cumulus parameterizations. In addition, the remaining trigger criteria in New SAS and SAS-based shallow cumulus were kept unchanged. Moreover, we use an updated version of the HCF trigger criterion, compared to that used in B015. The updated HCF trigger uses 2 m virtual potential temperature instead of 2 m potential temperature.

2.5. Statistical Significance

We evaluate the statistical significance of changes in model error resulting from the implementation of the HCF trigger using the methodology proposed by *DelSole and Tippett* [2014]. They showed that the traditional metrics for the evaluation of forecast skill could be too conservative. That is, these metrics may wrongly judge differences in forecast skill as insignificant. The authors proposed several ways of evaluating improvements in models using squared differences in combination to several statistical hypothesis tests. We use the Wilcoxon Signed-Rank Test [*Wilks*, 2006] as a metric to evaluate the statistical significance of all the results presented in this work.

3. Stand-alone Triggering Evaluation

Before investigating the impact of the HCF trigger in simulations, we tested the effect of the original SAS criterion and the HCF trigger on observed soundings. Both trigger criteria depend solely on the profiles of temperature and humidity. The other trigger criteria used in SAS require more information than just profiles of humidity and temperature. Therefore, the results shown in this section were obtained by turning off all the other trigger criteria in SAS. Results shown in subsequent sections were obtained with the other trigger criteria in SAS turned on.

Figure 2 shows a comparison between the HCFv2 trigger and the original SAS trigger (pressure difference) applied to temperature and humidity profiles from radiosonde data from the Dynamics of the Madden Julian Oscillation (DYNAMO) project [*Ciesielski et al*., 2014]. The skill scores were calculated considering all radiosondes available for the 28 locations listed in Figure 2d. The skill of each of the trigger criteria was evaluated based on the occurrence of convection using a two by two contingency table. Following the methodology used by *Suhas and Zhang* [2014] we used precipitation values as a proxy for convection. Instead of choosing a fixed threshold to characterize convective precipitation, we stratified the precipitation values. The precipitation thresholds in Figures 2a–2c are based on the average of four grid points from TRMM around the release time and location of each radiosonde.

We verify that the HCFv2 trigger performs better than the original SAS trigger as shown by the Heidke Skill Score (HSS—Figure 2a), the Equitable Threat Score (ETS—Figure 2b), and the bias

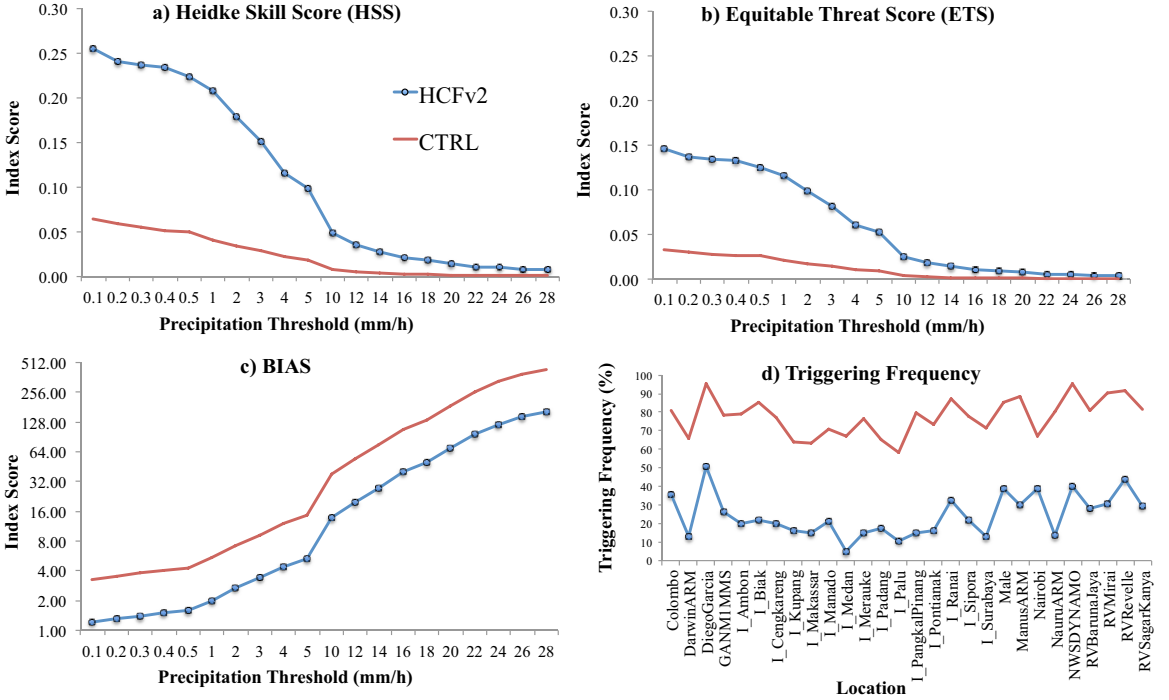

Figure 2. Comparison between the HCFv2 trigger and the original triggering (CTRL) mechanisms shown by (a) the Heidke Skill Score; (b) the Equitable Threat Score; (c) the Bias; and (d) the triggering frequency for each sounding release location.

(Figure 2c) (a brief description of these skill scores is presented in Appendix A). This result is mainly due to the fact that the original SAS trigger initiates convection too often (Figure 2d), resulting in a large number of false alarms.

However, it is worth mentioning that these results are related to only the first trigger criterion in the several triggering criteria used in SAS, such as a critical value of the cloud work function [e.g., *Lee et al*., 2008]. Therefore, the SAS trigger criteria in reality would not initiate convection as often as shown in Figure 2d. Nonetheless, the over-activation of convection is a known problem in SAS and a common error in most convective parameterizations [*Dai*, 2006; *Suhas and Zhang*, 2014].

4. Seasonal Simulations

Because the CFSv2 is an American model and the objective of the Monsoon Mission Project is to improve the seasonal forecast for the Indian monsoon, we will focus our analyses mostly over the United States (U.S.) and India. Figure 3 shows the lead-time spatial root-mean-square error (RMSE) of monthly mean precipitation for both CTRL and HCFv2 experiments in comparison to TRMM. We verify a reduction of monthly precipitation error over the western U.S. (Figures 3a and 3b) and over central India (Figures 3e and 3f). On the other hand, the HCF trigger results in an increase of monthly precipitation error over eastern U.S. (Figures 3c and 3d).

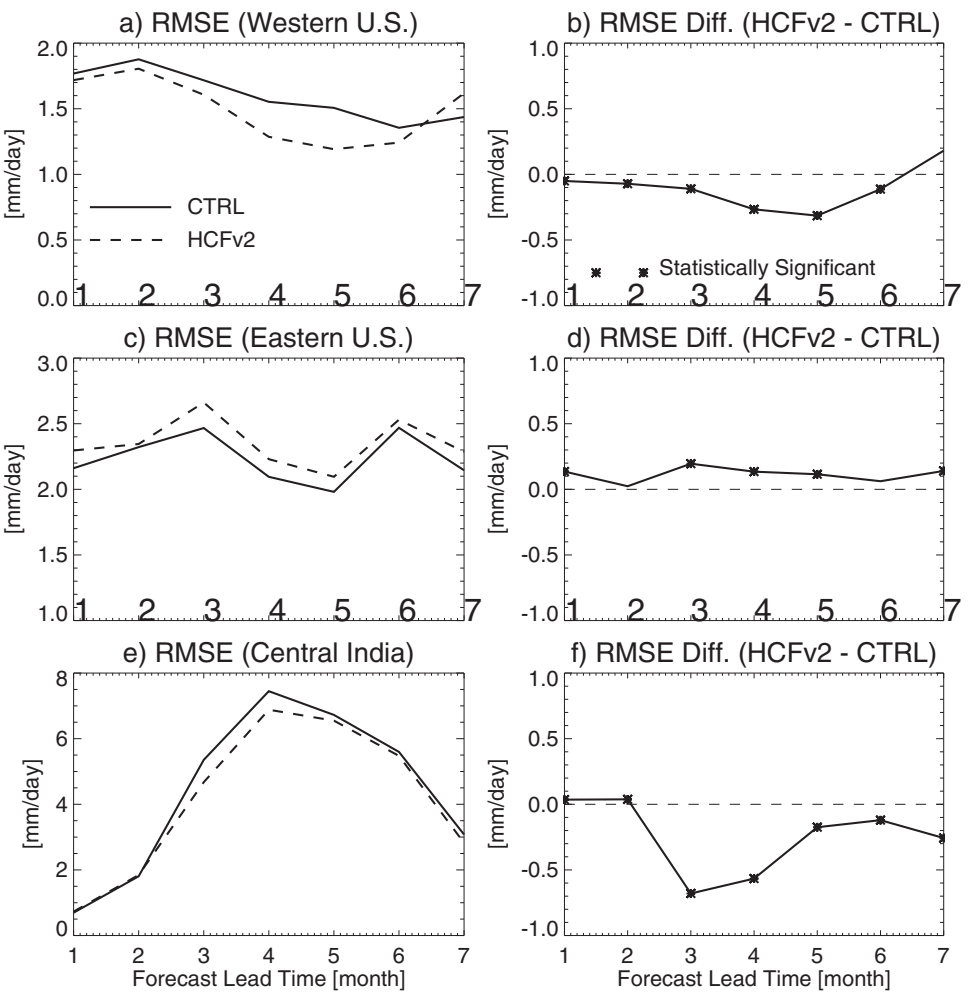

Figure 3. Spatial RMSE (mm/d) and RMSE difference (HCFv2 – CTRL) with respect to lead month for (a, b) Western U.S. (125.5°W–100.0°W; 31.5°N–49.5°N); (c, d) Eastern U.S. (100.0°W – 69.0°W; 31.5°N – 49.5°N); and (e, f) Central India (74.5°E–86.5°E; 16.5°N–26.5°N). The "*" indicates RMSE differences that are statistically significant at 5% level according to the Wilcoxon Signed-Rank Test of squared differences as described in *DelSole and Tippett* [2014].

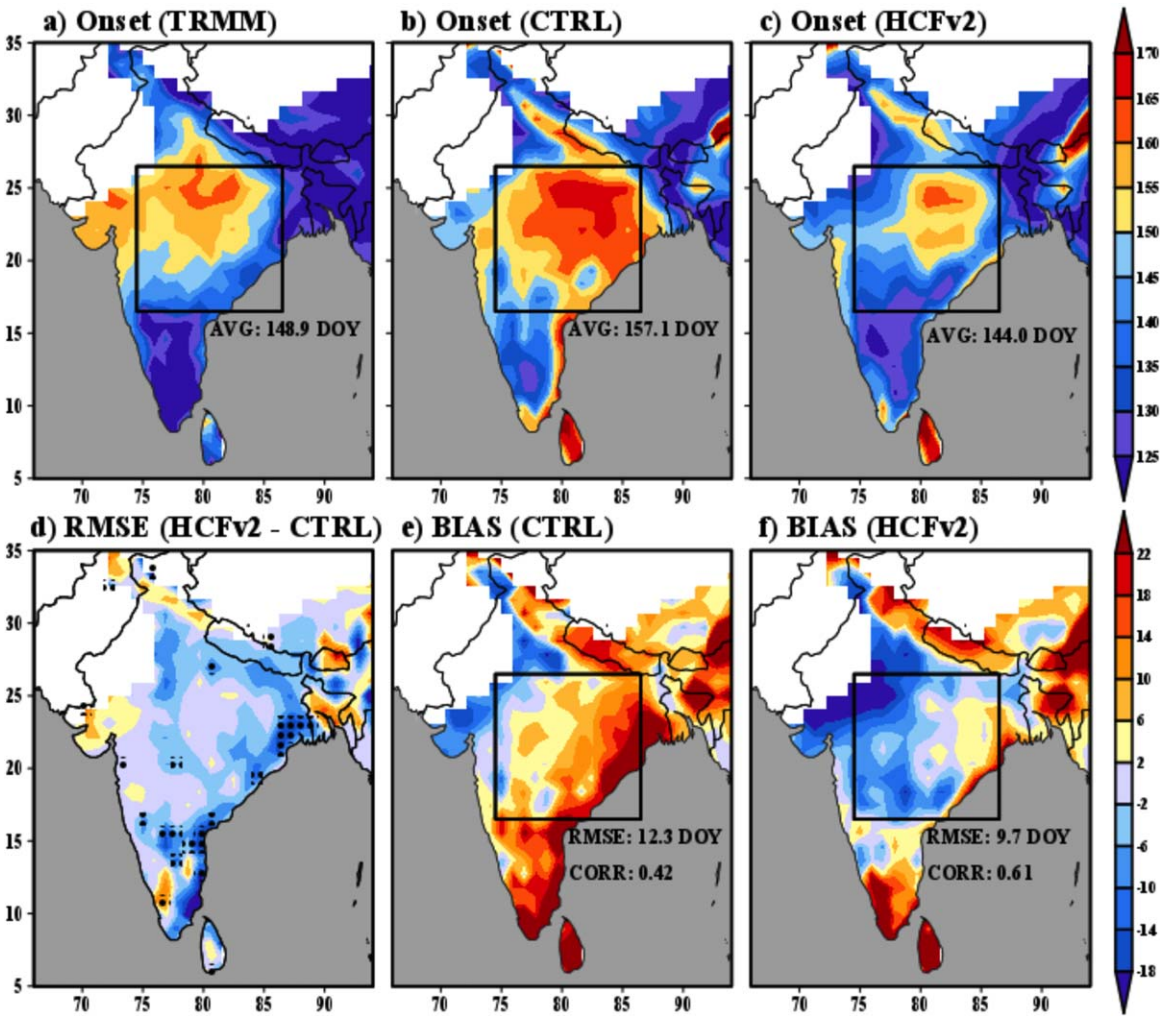

Figure 4. Rainy season onset dates (Day Of Year) for (a) Observations; (b) CTRL; (c) HCFv2. Onset date (d) RMSE difference (HCFv2 – CTRL) and onset date bias for (e) CTRL and (f) HCFv2. The stippling in Figure 4d indicates RMSE differences that are statistically significant at 5% level according to the Wilcoxon Signed-Rank Test of squared differences as described in *DelSole and Tippett* [2014].

The new trigger also has an impact on the onset dates of the rainy season over India. Figure 4 shows a comparison of the onset date of the rainy season over India between the numerical experiments and the TRMM precipitation data. The rainy season timing is calculated using a method based on *Liebmann and Marengo* [2001] that was further modified by *Bombardi and Carvalho* [2009]. The method depends only on precipitation (equation (3)):

$$S(t_n) = \sum_{i=0}^{n} [P(t_i) - P_C] \tag{3}$$

where S is the accumulated precipitation anomaly, P is the daily precipitation, and P_C is the annual climatological mean. The accumulated precipitation anomalies are computed for each grid point starting from the dry season (date of the minimum in the precipitation annual cycle, t_0) and up to one year (n ranges from 0 to the number of data in 1 year and t_n is any given day between t_0 and t_0 + one year). The S curve will initially have negative values. Once the precipitation becomes frequent, the S curve undergoes an inflection and starts to increase. After smoothing the S curve using a 1-2-1 filter, the onset of the rainy season is defined as the date when the first derivative of the smoothed S changes from negative to positive. This method was applied to each member of the seasonal simulations separately.

The onset date (Day Of Year – DOY) in the observations shows the northwestward progression of the Indian Summer Monsoon starting in early May (DOY 125) in the south, to early June (DOY 155) over central India,

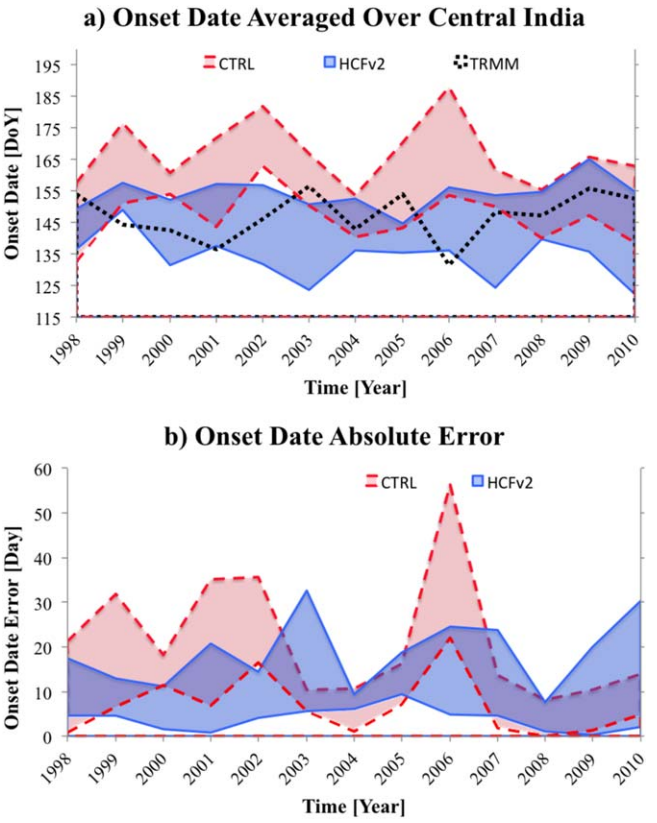

Figure 5. (a) Onset date averaged over Central India (74.5°E–86.5°E; 16.5°N–26.5°N). The graph shows the maximum and minimum values forecasted by each experiment. The dotted line shows the values from TRMM. b) Onset date absolute error. The graph shows the maximum and minimum absolute forecast error for each experiment in comparison to TRMM.

and up to mid June (DOY 165) over northwestern India (Figure 4a). These results are in agreement with the climatological values [e.g., *Joseph et al*., 1994; *Fasullo and Webster*, 2002]. The CTRL experiment does not realistically represent the northwestward evolution of the Indian Summer Monsoon (Figures 4b and 4e), a problem that was also found in the first version of the CFS model [*Yang et al*., 2008].

We find that the onset date of the rainy season is much closer to the observations in the HCFv2 than in CTRL (Figure 4c). The onset date error in HCFv2 tends to be equal or just slightly smaller than in CTRL (Figure 4d). However, there is a clear reduction in spatial RMSE and an increase in spatial correlation in HCFv2 in comparison to CTRL over central India (Figures 4e and 4f). There are no clear changes among experiments in the onset of the rainy season in other monsoonal regions such as North America, West Africa, and East Asia (not shown). It is also worth mentioning that we did not find any clear change in large-scale features of monsoon evolution around the time of onset such as midtropospheric temperature gradient and vertical wind shear (not shown).

Figure 5 shows the rainy season onset date forecast spread (Figure 5a) as well as the forecast error spread (Figure 5b) averaged over Central India for every year. HCFv2 onset date forecasts are closer to observations and show smaller amplitude than CTRL (Figure 5a). In addition, the forecast error (Figure 5b) tends to be smaller in HCFv2 than in CTRL.

Our attempts to investigate the mechanisms whereby the HCF trigger changes the rainy season onset timing over India were inconclusive. The CFSv2 is an operational model, which means that the output of all state variables is instantaneous. Therefore, we could only store the 00Z value for each simulation day in the seasonal runs. That means that we would only have state variable values for 5:30 am local time over India (see Sec. 6 for a detailed evaluation of the mechanisms associated with the HCF trigger).

5. The Diurnal Cycle of Precipitation

Although the CFSv2 is a climate model, it is reasonable to expect that effects of changing the convective trigger will also have impacts on shorter timescales. Therefore, the purpose of this section is to highlight the impact of the HCF trigger on the amplitude and phase of the diurnal cycle of precipitation (Diurnal Cycle runs). Since we are only interested in evaluating if the HCF trigger imposes any changes in the timing or intensity of convection, we define the diurnal cycle amplitude as simply the average of the range of the mean diurnal cycle and the phase as the local time of maximum peak precipitation in the mean diurnal cycle. A more rigorous analysis of the diurnal cycle involving the least-squares-fitted of the first (24 h) and second (12 h) harmonics can be found in *Chang et al*. [1995]; *Dai* [2001]; *Collier* [2004]; *Dai and Trenberth* [2004]; and *Pritchard and Somerville* [2009].

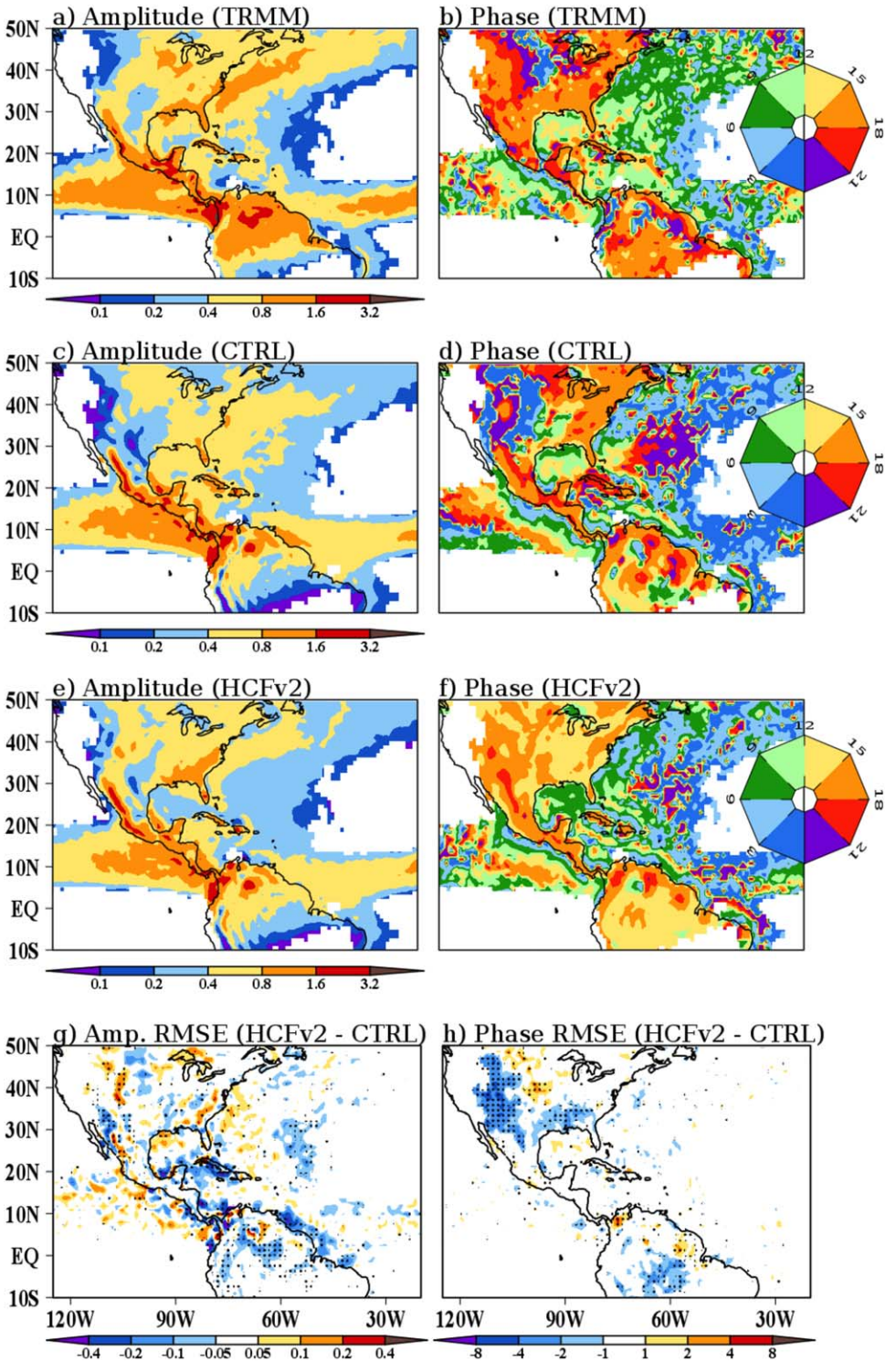

Figure 6. Mean amplitude of the diurnal cycle of precipitation (mm/3 h) for (a) TRMM, (c) CTRL, and (e) HCFv2. Mean phase (LST) of the diurnal cycle of precipitation for (b) TRMM, (d) CTRL, and (f) HCFv2. RMSE difference between HCFv2 and CTRL for g) amplitude and h) phase of the diurnal cycle of precipitation. We mask regions where the amplitude of the observed diurnal cycle is very weak (<0.1 mm/3h). The stippling in g-h indicates RMSE differences that are statistically significant at 5% level according to the Wilcoxon Signed-Rank Test of squared differences as described in *DelSole and Tippett* [2014].

The CFSv2 underestimates the amplitude of the diurnal cycle of precipitation over land (Figures 6a, 6c, and 6e) and there are no clear differences in the amplitude of the diurnal cycle of precipitation between HCFv2 and CTRL (Figure 6g). Even though the phase in the observations are representative only of the second half of July (Figure 6b), these results are consistent with the findings from observational studies of summertime diurnal cycle of precipitation [*Lee et al*., 2007b; *Kikuchi and Wang*, 2008; *Sahany et al*., 2010; *Biasutti et al*., 2012].

The phase is not very well represented by the CFSv2 (Figures 6b, 6d, and 6f), a common problem in climate models [e.g., *Bechtold et al*., 2004]. The largest phase differences between simulations and observations occur over the Great Plains in the U.S. (Figures 6b, 6d, and 6f), which has a maximum during nighttime (Figure 6c). The latter error is common in atmospheric models, because they do not accurately represent mesoscale convective complexes (MCS) that originate over the Rocky Mountains in early afternoon and propagate across the Great Plains over a period of several hours, which are responsible for most warm season rainfall in that region [*Fritsch et al*., 1986; *Dirmeyer et al*., 2012]. There is a remarkable difference between the phase simulated by CTRL and HCFv2 (Figures 6d and 6f). While CTRL simulates phases with maximum during nighttime over the Central U.S. (Figure 6d), the maximum precipitation simulated by HCFv2 falls during the afternoon (Figure 6f).

The largest impact of the HCF trigger in the phase of the diurnal cycle of precipitation is observed over the western U.S. (Figure 6h). *Tawfik et al*. [2015b] found that the HCF accurately identified the leeside of the Rocky Mountains as the primary triggering region. However, precipitation over the Great Plains is derived from the propagation of MCS from the lee of the Rocky Mountains toward the Great Plains. Therefore, it is not surprising that the HCF trigger did not improve the representation of the phase of the diurnal cycle

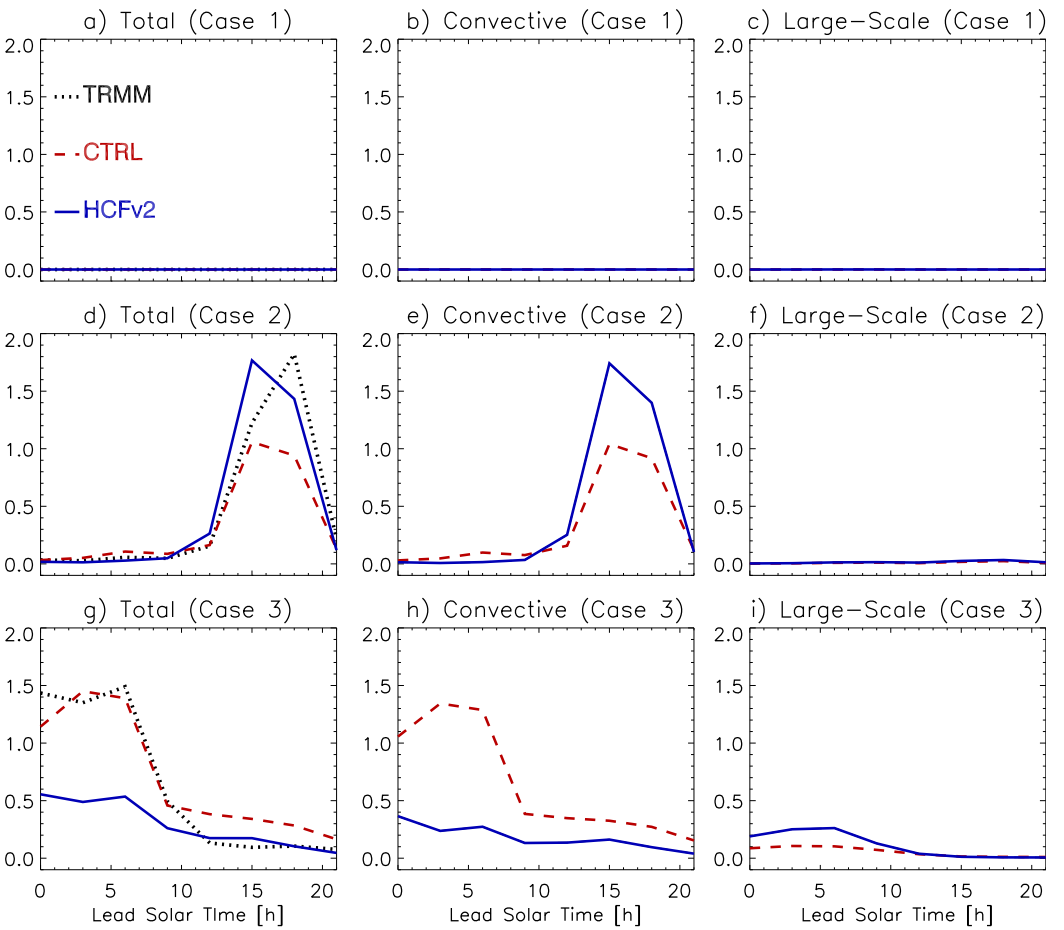

Figure 7. Diurnal cycle of (left) total precipitation, (middle) convective precipitation, and (right) large-scale precipitation for each type (Cases 1–3) of diurnal cycles.

over that region, as more events are triggered upwind of the Plains in the HCF and then treated in a column-based convective scheme, and therefore are not allowed to propagate after initiation (Figure 6h).

To further assess the model's performance over the Great Plains we evaluate the experiments representation of different types of diurnal cycles, similar to those studied by *Zhang and Klein* [2010]. Since their work focuses on spatial scales comparable to a single grid point of the CFSv2, we focused our analysis on a larger region in the southern Great Plains [105°W-95°W; 30°N-40°N]. In addition, we divided the different diurnal cycles into 3 categories instead of 4:

Case 1 – For the sake of simplicity, our first case is a combination of the first two cases studied by *Zhang and Klein* [2010], "clear skies" and "fair weather" without any consideration about cloud cover. These are cases with precipitation less than 0.1 mm d^{-1} at all times.
Case 2 – Late afternoon or early evening deep convection: Diurnal maximum hourly precipitation rate $\geq$ 1 mm d^{-1} occurring between 1500 and 2000 LST and being at least twice more than the precipitation rate at any other hour of the day outside of 1500–2000 LST (their case 3).
Case 3 – Nighttime deep convection: Diurnal maximum hourly precipitation rate $\geq$ 1 mm d^{-1} occurring between 0000 and 0700 LST (their case 4).

The partition of precipitation in the CFSv2 is dominated by convective precipitation; only a small fraction of the precipitation is due to large-scale precipitation (Figure 7). There is a clear improvement in the representation of late afternoon or early evening precipitation in the HCFv2 in comparison to CTRL (Figures 7d and

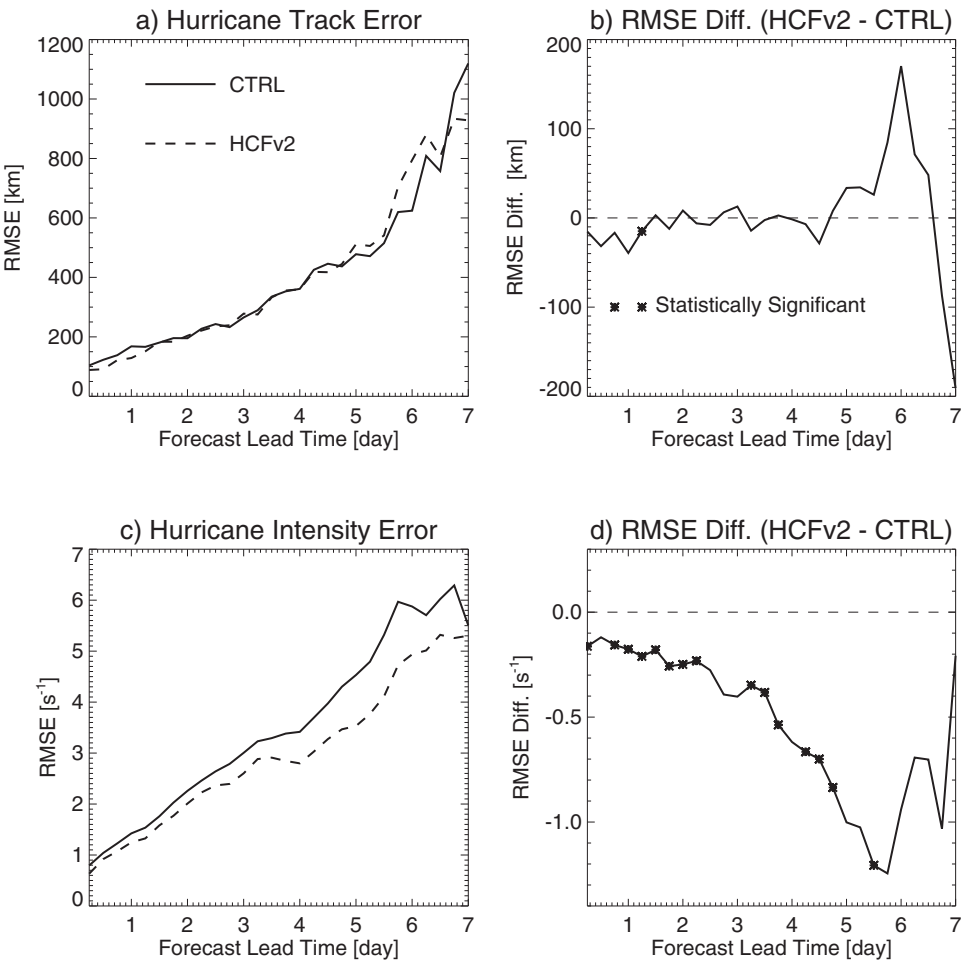

Figure 8. (a) Hurricane track RMSE with respect to lead days; (b) hurricane track RMSE difference between HCFv2 and CTRL; (c) hurricane intensity (vorticity) RMSE with respect to lead days; and (d) hurricane intensity RMSE difference between HCFv2 and CTRL. The RMSE is calculated against CFSR tracks. The "*" indicates RMSE differences that are statistically significant at 5% level according to the Wilcoxon Signed-Rank Test of squared differences as described in *DelSole and Tippett* [2014].

7e). On the other hand, nighttime deep convection is better represented by CTRL than HCFv2 (Figures 7g and 7h). Suggesting that the HCF trigger favors the delay of convection and, therefore, offers an advantage over CTRL for late afternoon or early evening precipitation (Case 2).

There were no significant differences in the representation of the phase or amplitude of the diurnal cycle of precipitation over India (not shown). In addition to the evaluation of the diurnal cycle of precipitation, we also evaluated the forecast skill and error of these short simulations, as defined by the lead-time anomaly correlation and anomaly root-mean-squared-error (RMSE) of 500hPa geopotential height. There was no clear difference in forecast skill or error between the two experiments over the extratropical Northern Hemisphere (20°N-80°N) or Southern Hemisphere (80°S-20°S) (not shown).

6. Tropical Cyclones

The representation of TCs is an important aspect of model physics for operational centers. Therefore, we test the impact of the HCF trigger in the representation of 24 hurricane events that made landfall (Table 2) using a higher horizontal resolution (T382; ∼38km) implementation of CFSv2.

Hurricane tracks are identified using a method similar to that used by *Bengtsson et al*. [2007] and based on the tracking algorithm of *Hodges* [1994, 1995, 1999]. Vortices are detected as maxima in the 6 hourly

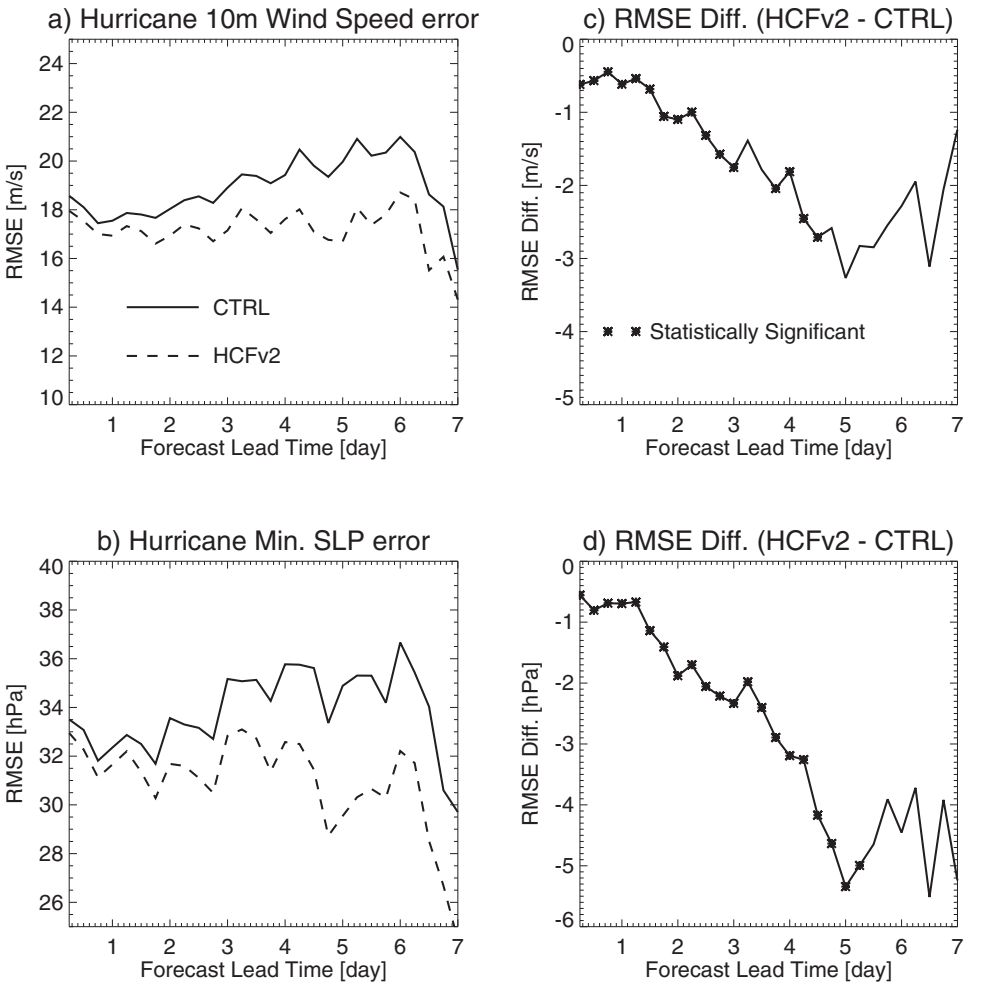

Figure 9. (a) Hurricane max 10 m wind speed RMSE with respect to lead days; (b) hurricane 10m speed RMSE difference between HCFv2 and CTRL; (c) hurricane minimum sea level pressure RMSE with respect to lead days; and (d) hurricane minimum sea level pressure RMSE difference between HCFv2 and CTRL. The RMSE is calculated against IBTrACS. The "*" indicates RMSE differences that are statistically significant at 5% level according to the Wilcoxon Signed-Rank Test of squared differences as described in *DelSole and Tippett* [2014].

relative vorticity field (averaged over 850, 700, and 650 hPa levels and truncated at a spectral resolution of T63) with values greater than 5×10^{-6} s^{-1}. Only events that last more than 2 days are considered.

The observed tracks (as in postseason best track data set, such as IBTrACS) are identified in the CFSR using track matching with IBTrACS following *Hodges et al*. [2011]. Tracks match if they overlap in time by any amount (accounting for differences in lifetimes between the IBTrACS and CFSR tracks), their mean separation is less than 4° geodesic, and are the track pair with minimum mean separation. This method achieves a high rate of identification of observed tracks in the analyses, with those missing being short-lived, weak systems [see *Hodges and Emerton*, 2015]. Likewise, to identify the same TCs in the forecast, the forecast tracks are matched against the CFSR tracks following a similar approach. Observed storms are identified in the analysis to provide extended verification lifecycles. As a result, model TCs tend to include both earlier and later stages of a life cycle than the observed storms.

When evaluating hurricane track intensity errors we compared simulations to the tracks calculated from CFSR (Figure 8). Location and intensity in both sets of tracks is based on lower-tropospheric vorticity. Error statistics based on this measure is shown to be consistent with more traditional verification metrics [see *Hodges and Emerton*, 2015]. In addition, 10 m wind speed and minimum sea level pressure (SLP) were compared against the IBTrACS (Figure 9) because these quantities are underestimated in the CFSR data due to the model's resolution [e.g., *Manganello et al*., 2012].

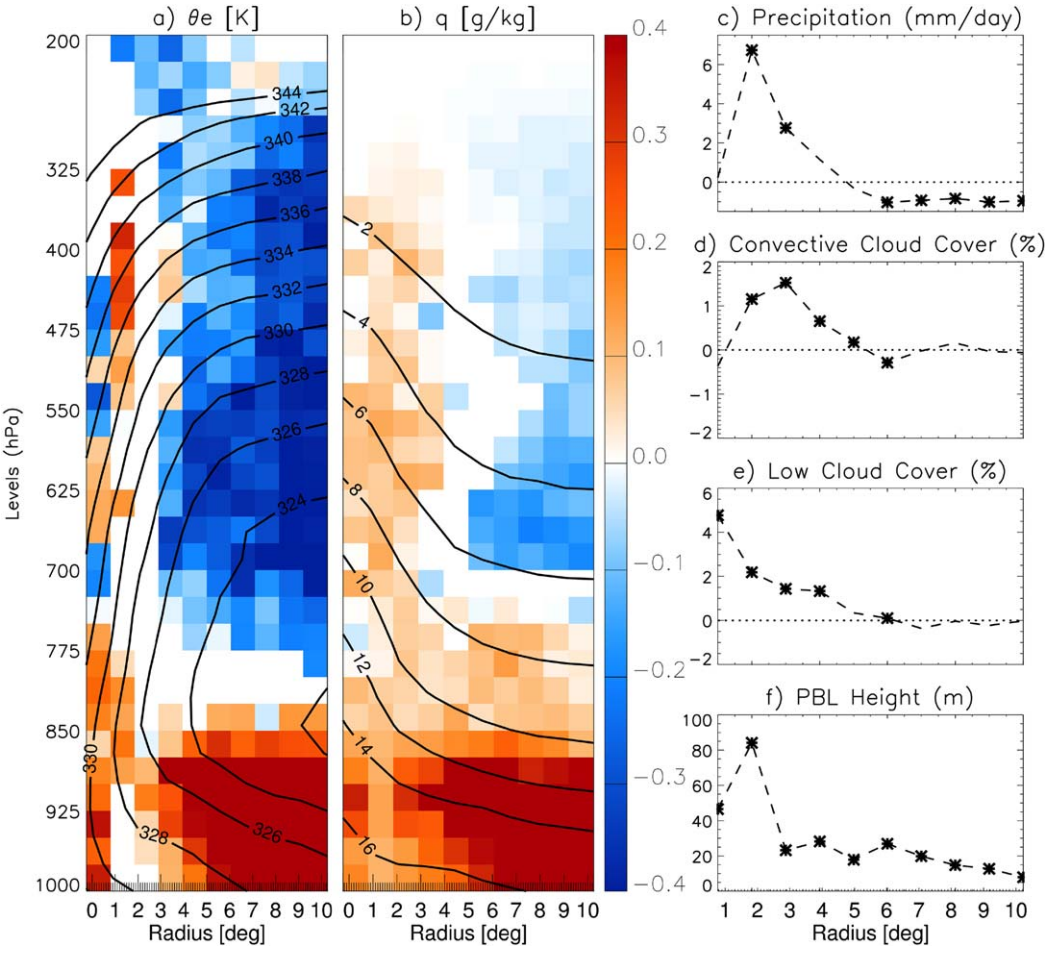

Figure 10. Median (CTRL; contours) and median difference (HCFv2 – CTRL; shading) of azimuthally averaged (a) equivalent potential temperature and (b) specific humidity. Median difference (HCFv2 – CTRL) of azimuthally averaged (c) precipitation (mm/3 h); (d) convective cloud cover (%); e) low cloud cover (%); and f) PBL height (m). Values averaged from 24 to 72 h of simulation. Shading or "*" indicates median differences that are statistically significant at 5% level according to the Wilcoxon Signed-Rank Test.

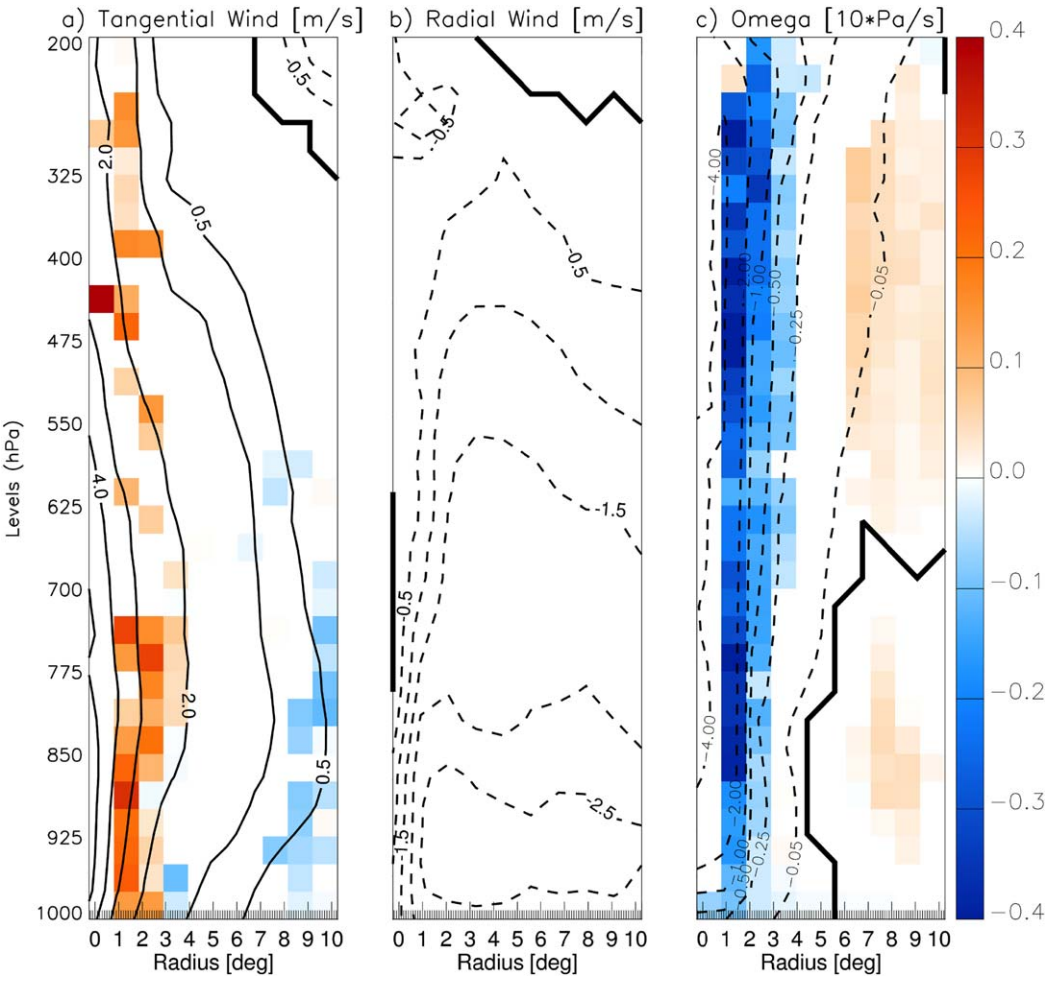

Figure 11. Median (CTRL; contours) and median difference (HCFv2 – CTRL; shading) of azimuthally averaged (a) tangential winds (m/s); (b) radial winds (m/s); and (c) omega (10 × Pa/s). Values averaged from 24 to 72 h of simulation. Shading indicates median differences that are statistically significant at 5% level according to the Wilcoxon Signed-Rank Test.

There is no clear improvement of hurricane tracks error in HCFv2 in comparison to CTRL (Figures 8a and 8b). On the other hand, the HCF trigger improves the representation of the intensity of hurricanes up to 5 days lead-time in terms of vorticity (Figures 8c and 8d), 10 m wind speed (Figures 9a and 9b), and minimum SLP (Figures 9c and 9d).

The hurricane tracking gave us a unique opportunity to follow these convective systems in order to investigate the mechanisms whereby the HCF trigger improves the representation of the intensity of hurricanes. Figures 10 and 11 show the median and the median difference of azimuthally averaged fields within 10° radius from the center of the hurricanes. We calculated averages in 1° bins and considering only the period from 24 to 72 h of simulation.

We verify that in comparison to CTRL the HCFv2 experiment shows a more convectively unstable atmosphere (Figure 10a), with increased moisture in the lower to middle troposphere (Figure 10b), increased precipitation close to the storm center and decreased precipitation away from the center of the storm (Figure 10c), increased convective (Figure 10d) and low cloud cover (Figure 10e), and increased PBL height (Figure 10f). The HCFv2 experiment also shows enhancements to the primary and secondary circulations: a slight increase in tangential wind in the lower troposphere (Figure 11a) in the TC core as well as increased upward velocity near the center and increased downward velocity away from the center (Figure 11c).

Overall, the HCF trigger causes a reduction in the activation of the convective schemes, increasing convective instability in comparison to CTRL. This allows the PBL to moisten and grow higher, injecting more

moisture into the lower to mid troposphere in HCFv2. The increase in atmospheric moisture is associated with an increase in precipitation, low and convective clouds, releasing latent heat and, consequently, increasing the hurricane intensity. These results are consistent with the findings of *Zadra et al*. [2014]. The trigger velocity is a constraint in the convective scheme of the GDPS. The authors reduced this parameter over the tropics, thus increasing the frequency of activation of the convective scheme. This increase in the convective activity led to a reduction of TC over prediction in terms of false alarm rate, due to a reduction of midlevel moisture, low-level convergence, and vorticity. Therefore, in CFSv2 a reduction in the frequency of convection led to the strengthening of TC intensity while in GDPS an increase in the frequency of convection led to a slight weakening of TC intensity.

This apparent inconsistency can be explained by the fact that although all coarse resolution models are expected to under predict TC intensity [*Wehner et al*., 2014], the GDPS had a tendency to overintensify TCs in comparison to other models [*Zadra et al*., 2014]. For this reason, *Zadra et al*. [2014] argue that the reduction in TC intensity in the GDPS does not necessarily mean a deterioration of forecast skill. It simply means the model generates TCs with intensities that are more comparable to the intensity generated by other models at that horizontal resolution. Nonetheless, the mechanisms whereby TC intensity is increased in the CFSv2 and decreased in the GDPS are consistent.

It is worth mentioning that there have been several studies on the representation of track and intensity of TCs using the high-resolution Hurricane Weather Research and Forecasting Model (HWRF) [*Gopalakrishnan et al*., 2012, 2013; *Biswas et al*., 2014; *Zhang and Marks*, 2015], including TC rapid intensification [*Kieu et al*., 2014; *Chen and Gopalakrishnan*, 2015]. Other factors related to the improvement of the representation of the intensity of TCs include: spatial resolution and initialization [*Gopalakrishnan et al*., 2012], the choice of physical parameterizations [*Ma and Tan*, 2009; *Gopalakrishnan et al*., 2012; *Biswas et al*., 2014], vertical diffusivity of both momentum and heat [*Gopalakrishnan et al*., 2013], and horizontal diffusion [*Zhang and Marks*, 2015].

7. Summary and Conclusions

This study is a follow-up study of B015 that studied the impact of implementing a new trigger (HCF) criterion into the parameterization of convection in the CFSv2. B015 introduced the HCF trigger as an additional criterion (maintaining the original criterion) to trigger the deep convection scheme (Old SAS) in the CFSv2. B015 observed an increase of summer Indian monsoon rainfall and an improvement of the representation of the onset date of the rainy season over India as a result of the implementation of the HCF trigger. In B015 the mechanism whereby the HCF trigger improved the representation of the rainy season over India was the fact that the convective scheme was allowed to trigger more often. By allowing the convective scheme to trigger more often, there was an increase in the amount of summer precipitation over India, which resulted in a reduction of the well-known dry bias over India. In this study, however, apart from using revised convective schemes (New SAS and SAS based shallow cumulus) in the CTRL experiments, the original trigger criterion of both deep and shallow convection were completely replaced by an updated version of the HCF trigger, which uses 2 m virtual potential temperature instead of 2 m potential temperature.

The HCF trigger outperforms the original trigger in SAS when applied to observed tropical soundings from the DYNAMO campaign. The improvement results from a reduction in convective initiation events (in contrast to B015) alleviating the high false alarm rate found in the original SAS triggering mechanism. It is worth mentioning that the SAS trigger function is based on several criteria. In this paper we investigate the impact of changing only the initial criterion.

On seasonal timescales, the HCF trigger improves the summer precipitation over the western U.S. and over India, including improvements in the onset date of the rainy season over India. However, there is an increase in precipitation error over the eastern U.S. The impact of the HCF trigger on the amplitude and phase of the diurnal cycle of precipitation is small and improvements were observed mostly over regions with weak diurnal cycle amplitude.

The mechanisms whereby the HCF trigger improves the representation of the intensity of hurricanes seems to be due to the fact that the HCF triggers convection less often than the original criterion, the convective scheme adjusts the atmospheric profiles less frequently, leaving the atmosphere in a more convectively unstable condition. This allows the PBL to grow and to inject more moisture into the lower troposphere.

The accumulation of moisture results in the increase of precipitation, low and convective clouds, releasing latent heat and, consequently, intensifying the hurricanes. This is consistent with *Han and Pan* [2011] regarding the fact that SAS initiates too frequently, removing cloud water from the middle troposphere through rainfall and injecting cloud water into upper troposphere by increased mixing and vertical motion.

Although the HCF trigger shows some improvements in the representation of convection in the CFSv2, the model still has large precipitation biases on seasonal timescales. The CFSv2 tends to overestimate precipitation over the ocean and underestimate it over land, even at higher spatial resolution [*Abhik et al*., 2015]. Part of this problem is because some atmospheric processes in the shallow and deep convection schemes are treated differently over land than over the ocean. The implementation of the HCF trigger in the shallow convection scheme eliminates the discrepancy in the initiation of shallow convection between land and ocean. However, the convective trigger criteria in the deep convection scheme (SAS) are more complex than that in the shallow convection scheme. SAS uses the Cloud Work Function (CWF) to determine the strength of convection [*Arakawa and Schubert*, 1974; *Lee et al*., 2008]. The CWF is a metric of atmospheric stability and in the SAS scheme the CWF has to reach a critical value in order for convection to occur. The CWF critical value which gives the best performance in the model depends on a convective adjustment timescale [*Moorthi and Suarez*, 1992] that assumes different values over land and ocean and is also highly dependent on the pressure difference in the original initial trigger criterion in the SAS scheme. This relationship between the initial and the CWF criteria might be related to the fact that the New SAS improved the forecast skill and the representation of convection in the CFSv2, but it also increased the surface temperature bias in comparison to Old SAS [*Han and Pan*, 2011]. Sensitivity tests (not shown here) verified that the CWF critical value could be tuned to the HCF trigger (as it is adjusted to the initial trigger criterion in the operational version of the model) to improve the forecast skill over the NINO3.4 region. However, tuning the convective scheme is outside the scope of this work. Additionally, a new cloud base mass flux calculation is already being developed in the SAS routine (J. Han, personal communication, 2015), and it is expected to eliminate the discrepancy in the CWF criterion between land and ocean in the deep convection scheme.

Since the HCF convective trigger shows improvements in the representation of convection in the CFSv2 and considering that the HCF is physically based on the balance between large-scale and surface flux destabilization as opposed to the pressure difference triggering criterion in SAS, this method holds promise for future operational prediction systems. Therefore, from a model development perspective, the implementation of the HCF trigger might be a good option for the SAS scheme in the CFSv2, especially when combined with planned improvements in the representation of the vertical profile of cloud condensate [e.g., *Hazra et al*., 2016; *De et al*., 2015] and the role of hydrometeors [e.g., *Halder et al*., 2012].

Appendix A: Forecast Skill Scores

A two by two contingency table is constructed in a way where "a" is the number of observed events that were correctly forecasted, "b" is the number events forecasted to occur but were not observed, "c" is the number of observed events that were not forecasted, "d" is the number of events that did not occur and were not forecasted, and n is total number of points (sum of a, b, c, and d). From this table, a number of forecast skill scores can be calculated. The Heidke Skill Score (HSS) is a measure of the proportion of correct forecasts that would be achieved by random forecasts that are statically independent of the observations (equation (A1)). Hence, perfect forecasts receive HSS = 1, forecasts equivalent to the reference forecast receive HSS = 0, and forecasts worse than the reference forecast receive negative scores [*Wilks*, 2006].

$$HSS = \frac{2(ad-bc)}{(a+c)(c+d)+(a+b)(b+d)} \tag{A1}$$

The Equitable Threat Score (ETS) is a score that is particularly useful when the event being forecasted occurs much less frequently than its nonoccurrence (equation (A2)). The ETS ranges form 0 to 1, where perfect forecasts receive ETS = 1 [*Wilks*, 2006].

$$ETS = \frac{(a-(a+b)(a+c)/n)}{a+b+c-[(a+b)(a+c)/n]} \tag{A2}$$

Likewise, the Bias can be calculates as equation (A3).

$$Bias = \frac{a+b}{a+c} \quad \text{(A3)}$$

Acknowledgments
This study is primarily supported by the National Monsoon Mission, Ministry of Earth Sciences, Government of India. Additional support comes from NSF (AGS-1338427), NOAA (NA14OAR4310160 and NA15NWS4680018) and NASA (NNX14AM19G). Rodrigo Bombardi thanks Dr. Timothy DelSole for his help with statistical tests. We thank the two anonymous reviewers for their suggestions for the improvement of this manuscript. In addition, we thank the European Centre for Medium-Range Weather Forecasts (ECMWF) for making available the ERA-interim reanalysis and the National Aeronautics and Space Administration (NASA) for making available the TRMM analysis. This work used the Extreme Science and Engineering Discovery Environment (XSEDE), which is supported by National Science Foundation grant ACI-1053575. Computing resources (ark:/85065/d7wd3xhc) were provided by the Climate Simulation Laboratory at NCAR's *Computational and Information Systems Laboratory* [2012], sponsored by the National Science Foundation and other agencies. The radiosonde data were collected as part of DYNAMO, which was sponsored by NSF, NOAA, ONR, DOE, NASA, JAMSTEC (Indian and Australian funding agencies). The involvement of the NSF-sponsored National Center for Atmospheric Research (NCAR) Earth Observing Laboratory (EOL) is acknowledged. The data are archived at the DYNAMO Data Archive Center maintained by NCAR EOL.

References

Abhik, S., P. Mukhopadhyay, R. P. M. Krishna, K. D. Salunke, A. R. Dhakate, and S. A. Rao (2015), Diagnosis of boreal summer intraseasonal oscillation in high resolution NCEP climate forecast system, *Clim. Dyn.*, *46*(9-10), 3287–3303, doi:10.1007/s00382-015-2769-9.

Arakawa, A., and W. H. Schubert (1974), Interaction of a cumulus cloud ensemble with the large-scale environment, Part I, *J. Atmos. Sci.*, *31*(3), 674–701, doi:10.1175/1520-0469(1974)031 <0674:IOACCE>2.0.CO;2.

Bacmeister, J. T., M. F. Wehner, R. B. Neale, A. Gettelman, C. Hannay, P. H. Lauritzen, J. M. Caron, and J. E. Truesdale (2014), Exploratory high-resolution climate simulations using the Community Atmosphere Model (CAM), *J. Clim.*, *27*(9), 3073–3099, doi:10.1175/JCLI-D-13-00387.1.

Bechtold, P., J.-P. Chaboureau, A. Beljaars, A. K. Betts, M. Köhler, M. Miller, and J.-L. Redelsperger (2004), The simulation of the diurnal cycle of convective precipitation over land in a global model, *Q. J. R. Meteorol. Soc.*, *130*(604), 3119–3137, doi:10.1256/qj.03.103.

Bengtsson, L., K. I. Hodges, and M. Esch (2007), Tropical cyclones in a T159 resolution global climate model: Comparison with observations and re-analyses, *Tellus, Ser. A*, *59 A*(4), 396–416, doi:10.1111/j.1600-0870.2007.00236.x.

Biasutti, M., S. E. Yuter, C. D. Burleyson, and A. H. Sobel (2012), Very high resolution rainfall patterns measured by TRMM precipitation radar: Seasonal and diurnal cycles, *Clim. Dyn.*, *39*(1-2), 239–258, doi:10.1007/s00382-011-1146-6.

Biswas, M. K., L. Bernardet, and J. Dudhia (2014), Sensitivity of hurricane forecasts to cumulus parameterizations in the HWRF model, *Geophys. Res. Lett.*, *41*, 9113–9119, doi:10.1002/2014GL062071.

Bombardi, R. J., and L. M. V. Carvalho (2009), IPCC global coupled model simulations of the South America monsoon system, *Clim. Dyn.*, *33*(7-8), 893–916, doi:10.1007/s00382-008-0488-1.

Bombardi, R. J., E. K. Schneider, L. Marx, S. Halder, B. Singh, A. B. Tawfik, P. a. Dirmeyer, and J. L. Kinter (2015), Improvements in the representation of the Indian summer monsoon in the NCEP climate forecast system version 2, *Clim. Dyn.*, *45*(9-10), 2485–2498, doi:10.1007/s00382-015-2484-6.

Chang, A. T. C., L. S. Chiu, and G. Yang (1995), Diurnal Cycle of Oceanic Precipitation from SSM/I Data, *Mon. Weather Rev.*, *123*(11), 3371–3380, doi:10.1175/1520-0493(1995)123 <3371:DCOOPF>2.0.CO;2.

Chao, W. C. (2013), Catastrophe-concept-based cumulus parameterization: Correction of systematic errors in the precipitation diurnal cycle over land in a GCM, *J. Atmos. Sci.*, *70*(11), 3599–3614, doi:10.1175/JAS-D-13-022.1.

Chen, H., and S. G. Gopalakrishnan (2015), A study on the asymmetric rapid intensification of Hurricane Earl (2010) using the HWRF system, *J. Atmos. Sci.*, *72*(2), 531–550, doi:10.1175/JAS-D-14-0097.1.

Chen, J.-H., and S.-J. Lin (2011), The remarkable predictability of inter-annual variability of Atlantic hurricanes during the past decade, *Geophys. Res. Lett.*, *38*, L11804, doi:10.1029/2011GL047629.

Ciesielski, P. E. et al. (2014), Quality-controlled upper-air sounding dataset for DYNAMO/CINDY/AMIE: Development and corrections, *J. Atmos. Oceanic Technol.*, *31*(4), 741–764, doi:10.1175/JTECH-D-13-00165.1.

Collier, J. C. (2004), Diurnal cycle of tropical precipitation in a general circulation model, *J. Geophys. Res.*, *109*, D17105, doi:10.1029/2004JD004818.

Computational and Information Systems Laboratory (2012), *Yellowstone: IBM iDataPlex System (Climate Simulation Laboratory)*, Natl. Cent. Atmos. Res., Boulder, Colo. [Available at http://n2t.net/ark:/85065/d7wd3xhc.]

Dai, A. (2001), Global precipitation and thunderstorm frequencies. Part II: Diurnal variations, *J. Clim.*, *14*(6), 1112–1128, doi:10.1175/1520-0442(2001)014 <1112:GPATFP>2.0.CO;2.

Dai, A. (2006), Precipitation characteristics in eighteen coupled climate models, *J. Clim.*, *19*(18), 4605–4630, doi:10.1175/JCLI3884.1.

Dai, A., and K. E. Trenberth (2004), The diurnal cycle and its depiction in the Community Climate System Model, *J. Clim.*, *17*(5), 930–951, doi:10.1175/1520-0442(2004)017 <0930:TDCAID>2.0.CO;2.

De, S., A. Hazra, and H. S. Chaudhari (2015), Does the modification in "critical relative humidity" of NCEP CFSv2 dictate Indian mean summer monsoon forecast? Evaluation through thermodynamical and dynamical aspects, *Clim. Dyn.*, *46*(3-4), 1197–1222, doi:10.1007/s00382-015-2640-z.

DelSole, T., and M. K. Tippett (2014), Comparing forecast skill, *Mon. Weather Rev.*, *142*(12), 4658–4678, doi:10.1175/MWR-D-14-00045.1.

Dirmeyer, P. A., et al. (2012), Simulating the diurnal cycle of rainfall in global climate models: Resolution versus parameterization, *Clim. Dyn.*, *39*(1-2), 399–418, doi:10.1007/s00382-011-1127-9.

Ek, M. B., K. E. Mitchell, Y. Lin, E. Rogers, P. Grunmann, V. Koren, G. Gayno, and J. D. Tarpley (2003), Implementation of Noah land surface model advances in the National Centers for Environmental Prediction operational mesoscale Eta model, *J. Geophys. Res.*, *108*(D22), 8851, doi:10.1029/2002JD003296.

Fasullo, J., and P. J. Webster (2002), Hydrological signatures relating the asian summer monsoon and ENSO, *J. Clim.*, *15*(21), 3082–3095, doi:10.1175/1520-0442(2002)015 <3082:HSRTAS>2.0.CO;2.

Fritsch, J. M., R. J. Kane, and C. R. Chelius (1986), The contribution of mesoscale convective weather systems to the warm-season precipitation in the United States, *J. Clim. Appl. Meteorol.*, *25*(10), 1333–1345, doi:10.1175/1520-0450(1986)025 <1333:TCOMCW>2.0.CO;2.

Ganai, M., P. Mukhopadhyay, R. P. M. Krishna, and M. Mahakur (2015), The impact of revised simplified Arakawa–Schubert convection parameterization scheme in CFSv2 on the simulation of the Indian summer monsoon, *Clim. Dyn.*, *45*(3-4), 881–902, doi:10.1007/s00382-014-2320-4.

Gopalakrishnan, S. G., S. Goldenberg, T. Quirino, X. Zhang, F. Marks, K.-S. Yeh, R. Atlas, and V. Tallapragada (2012), Toward improving high-resolution numerical hurricane forecasting: Influence of model horizontal grid resolution, initialization, and physics, *Weather Forecasting*, *27*(3), 647–666, doi:10.1175/WAF-D-11-00055.1.

Gopalakrishnan, S. G., F. Marks, J. A. Zhang, X. Zhang, J.-W. Bao, and V. Tallapragada (2013), A Study of the impacts of vertical diffusion on the structure and intensity of the tropical cyclones using the high-resolution HWRF system, *J. Atmos. Sci.*, *70*(2), 524–541, doi:10.1175/JAS-D-11-0340.1.

Grabowski, W. W. (2001), Coupling Cloud processes with the large-scale dynamics using the Cloud-Resolving Convection Parameterization (CRCP), *J. Atmos. Sci.*, *58*(9), 978–997, doi:10.1175/1520-0469(2001)058 <0978:CCPWTL>2.0.CO;2.

Griffies, S. M., M. J. Harrison, R. C. Pacanowski, and A. Rosati (2004), A technical guide to MOM4, *GFDL Ocean Group Tech. Rep. 5.* [Available at http://www.gfdl.noaa.gov.]

Halder, M., P. Mukhopadhyay, and S. Halder (2012), Study of the microphysical properties associated with the Monsoon Intraseasonal Oscillation as seen from the TRMM observations, *Ann. Geophys.*, *30*(6), 897–910, doi:10.5194/angeo-30-897-2012.

Han, J., and H.-L. Pan (2011), Revision of convection and vertical diffusion schemes in the NCEP Global Forecast System, *Weather Forecasting*, *26*(4), 520–533, doi:10.1175/WAF-D-10-05038.1.

Hazra, A., H. S. Chaudhari, and A. Dhakate (2016), Evaluation of cloud properties in the NCEP CFSv2 model and its linkage with Indian summer monsoon, *Theor. Appl. Climatol.*, *124*(1-2), 31–41, doi:10.1007/s00704-015-1404-3.

Hodges, K. I. (1994), A general method for tracking analysis and its application to meteorological data, *Mon. Weather Rev.*, *122*(11), 2573–2586, doi:10.1175/1520-0493(1994)122 <2573:AGMFTA>2.0.CO;2.

Hodges, K. I. (1995), Feature tracking on the unit sphere, *Mon. Weather Rev.*, *123*(12), 3458–3465, doi:10.1175/1520-0493(1995)123 <3458:FTOTUS>2.0.CO;2.

Hodges, K. I. (1999), Adaptive constraints for feature tracking, *Mon. Weather Rev.*, *127*(6), 1362–1373, doi:10.1175/1520-0493(1999)*127*<1362:ACFFT>2.0.CO;2.

Hodges, K. I., and R. Emerton (2015), The prediction of northern hemisphere tropical cyclone extended life cycles by the ECMWF ensemble and deterministic prediction systems. Part I: Tropical cyclone stage*, *Mon. Weather Rev.*, *143*(12), 5091–5114, doi:10.1175/MWR-D-13-00385.1.

Hodges, K. I., R. W. Lee, and L. Bengtsson (2011), A comparison of extratropical cyclones in recent reanalyses ERA-Interim, NASA MERRA, NCEP CFSR, and JRA-25, *J. Clim.*, *24*(18), 4888–4906, doi:10.1175/2011JCLI4097.1.

Hong, S.-Y., and H.-L. Pan (1998), Convective trigger function for a mass-flux cumulus parameterization scheme, *Mon. Weather Rev.*, *126*, 2599–2620.

Huffman, G. J., D. T. Bolvin, E. J. Nelkin, D. B. Wolff, R. F. Adler, G. Gu, Y. Hong, K. P. Bowman, and E. F. Stocker (2007), The TRMM Multisatellite Precipitation Analysis (TMPA): Quasi-global, multiyear, combined-sensor precipitation estimates at fine scales, *J. Hydrometeorol.*, *8*(1), 38–55, doi:10.1175/JHM560.1.

Joseph, P. V., J. K. Eischeid, and R. J. Pyle (1994), Interannual variability of the onset of the indian summer monsoon and its association with atmospheric features, El Niño, and sea surface temperature anomalies, *J. Clim.*, *7*(1), 81–105, doi:10.1175/1520-0442(1994)007 <0081:IVOTOO>2.0.CO;2.

Khairoutdinov, M. F., and D. A. Randall (2001), A cloud resolving model as a cloud parameterization in the NCAR Community Climate System Model: Preliminary results, *Geophys. Res. Lett.*, *28*(18), 3617–3620, doi:10.1029/2001GL013552.

Kieu, C., V. Tallapragada, and W. Hogsett (2014), Vertical structure of tropical cyclones at onset of the rapid intensification in the HWRF model, *Geophys. Res. Lett.*, *41*, 3298–3306, doi:10.1002/2014GL059584.

Kikuchi, K., and B. Wang (2008), Diurnal precipitation regimes in the global tropics*, *J. Clim.*, *21*(11), 2680–2696, doi:10.1175/2007JCLI2051.1.

Knapp, K. R., M. C. Kruk, D. H. Levinson, H. J. Diamond, and C. J. Neumann (2010), The International Best Track Archive for Climate Stewardship (IBTrACS), *Bull. Am. Meteorol. Soc.*, *91*(3), 363–376, doi:10.1175/2009BAMS2755.1.

Lee, M.-I., S. D. Schubert, M. J. Suarez, I. M. Held, N.-C. Lau, J. J. Ploshay, A. Kumar, H.-K. Kim, and J.-K. E. Schemm (2007a), An analysis of the warm-season diurnal cycle over the continental United States and Northern Mexico in general circulation models, *J. Hydrometeorol.*, *8*(3), 344–366, doi:10.1175/JHM581.1.

Lee, M.-I., S. D. Schubert, M. J. Suarez, T. L. Bell, and K.-M. Kim (2007b), Diurnal cycle of precipitation in the NASA Seasonal to Interannual Prediction Project atmospheric general circulation model, *J. Geophys. Res.*, *112*, D16111, doi:10.1029/2006JD008346.

Lee, M.-I., S. D. Schubert, M. J. Suarez, J.-K. E. Schemm, H.-L. Pan, J. Han, and S.-H. Yoo (2008), Role of convection triggers in the simulation of the diurnal cycle of precipitation over the United States Great Plains in a general circulation model, *J. Geophys. Res.*, *113*, D02111, doi:10.1029/2007JD008984.

Liebmann, B., and J. A. Marengo (2001), Interannual variability of the rainy season and rainfall in the Brazilian Amazon Basin, *J. Clim.*, *14*(22), 4308–4318, doi:10.1175/1520-0442(2001)014 <4308:IVOTRS>2.0.CO;2.

Lin, J. L., M. I. Lee, D. Kim, I. S. Kang, and D. M. W. Frierson (2008), The impacts of convective parameterization and moisture triggering on AGCM-simulated convectively coupled equatorial waves, *J. Clim.*, *21*(5), 883–909, doi:10.1175/2007JCLI1790.1.

Ma, L. M., and Z. M. Tan (2009), Improving the behavior of the cumulus parameterization for tropical cyclone prediction: Convection trigger, *Atmos. Res.*, *92*(2), 190–211, doi:10.1016/j.atmosres.2008.09.022.

Manganello, J. V., et al. (2012), Tropical cyclone climatology in a 10-km global atmospheric GCM: Toward weather-resolving climate modeling, *J. Clim.*, *25*(11), 3867–3893, doi:10.1175/JCLI-D-11-00346.1.

Moorthi, S., and M. J. Suarez (1992), Relaxed Arakawa-Schubert. A parameterization of moist convection for general circulation models, *Mon. Weather Rev.*, *120*(6), 978–1002, doi:10.1175/1520-0493(1992)120 <0978:RASAPO>2.0.CO;2.

Murakami, H., et al. (2012), Future changes in tropical cyclone activity projected by the new high-resolution MRI-AGCM*, *J. Clim.*, *25*(9), 3237–3260, doi:10.1175/JCLI-D-11-00415.1.

Pan, H.-L., and W.-S. Wu (1995), Implementing a mass flux convective parameterization package for the NMC medium range forecast model, *NMC Off. Note 409*, 40 pp. [Available at http://www.emc.ncep.no.]

Pezza, A. B. (2005), The first South Atlantic hurricane: Unprecedented blocking, low shear and climate change, *Geophys. Res. Lett.*, *32*, L15712, doi:10.1029/2005GL023390.

Pritchard, M. S., and R. C. J. Somerville (2009), Assessing the diurnal cycle of precipitation in a multi-scale climate model, *J. Adv. Model. Earth Syst.*, *2*, 12, doi:10.3894/JAMES.2009.1.12.

Randall, D., M. Khairoutdinov, A. Arakawa, and W. Grabowski (2003), Breaking the Cloud Parameterization Deadlock, *Bull. Am. Meteorol. Soc.*, *84*(11), 1547–1564, doi:10.1175/BAMS-84-11-1547.

Reynolds, R. W., T. M. Smith, C. Liu, D. B. Chelton, K. S. Casey, and M. G. Schlax (2007), Daily high-resolution-blended analyses for sea surface temperature, *J. Clim.*, *20*(22), 5473–5496, doi:10.1175/2007JCLI1824.1.

Saha, S., et al. (2010), The NCEP climate forecast system reanalysis, *Bull. Am. Meteorol. Soc.*, *91*(8), 1015–1057, doi:10.1175/2010BAMS3001.1.

Saha, S., et al. (2014), The NCEP climate forecast system version 2, *J. Clim.*, *27*(6), 2185–2208, doi:10.1175/JCLI-D-12-00823.1.

Sahany, S., V. Venugopal, and R. S. Nanjundiah (2010), Diurnal-scale signatures of monsoon rainfall over the Indian region from TRMM satellite observations, *J. Geophys. Res.*, *115*, D02103, doi:10.1029/2009JD012644.

Satoh, M., T. Matsuno, H. Tomita, H. Miura, T. Nasuno, and S. Iga (2008), Nonhydrostatic icosahedral atmospheric model (NICAM) for global cloud resolving simulations, *J. Comput. Phys.*, *227*(7), 3486–3514, doi:10.1016/j.jcp.2007.02.006.

Satoh, M., et al. (2014), The Non-hydrostatic Icosahedral Atmospheric Model: Description and development, *Prog. Earth Planet. Sci.*, *1*(1), 18, doi:10.1186/s40645-014-0018-1.

Silva, C. M. S. E., and S. R. de Freitas (2015), Impacto de um mecanismo de disparo da convecção na precipitação simulada com o modelo regional BRAMS sobre a bacia amazônica durante a estação chuvosa de 1999, *Rev. Bras. Meteorol.*, *30*(2), 145–157, doi:10.1590/0102-778620140039.

Stan, C., M. Khairoutdinov, C. A. DeMott, V. Krishnamurthy, D. M. Straus, D. A. Randall, J. L. Kinter, and J. Shukla (2010), An ocean-atmosphere climate simulation with an embedded cloud resolving model, *Geophys. Res. Lett.*, *37*, L01702, doi:10.1029/2009GL040822.

Suhas, E., and G. J. Zhang (2014), Evaluation of trigger functions for convective parameterization schemes using observations, *J. Clim.*, *27*(20), 7647–7666, doi:10.1175/JCLI-D-13-00718.1.

Tawfik, A. B., and P. A. Dirmeyer (2014), A process-based framework for quantifying the atmospheric preconditioning of surface-triggered convection, *Geophys. Res. Lett.*, *41*, 173–178, doi:10.1002/2013GL057984.

Tawfik, A. B., P. A. Dirmeyer, and J. A. Santanello (2015a), The heated condensation framework. Part I: Description and Southern Great Plains case study, *J. Hydrometeorol.*, *16*(5), 1929–1945, doi:10.1175/JHM-D-14-0117.1.

Tawfik, A. B., P. A. Dirmeyer, and J. A. Santanello (2015b), The heated condensation framework. Part II: Climatological behavior of convective initiation and land-atmosphere coupling over the Conterminous United States, *J. Hydrometeorol.*, *16*(5), 1946–1961, doi:10.1175/JHM-D-14-0118.1.

Tomita, H., and M. Satoh (2004), A new dynamical framework of nonhydrostatic global model using the icosahedral grid, *Fluid Dyn. Res.*, *34*(6), 357–400, doi:10.1016/j.fluiddyn.2004.03.003.

Wang, W., and M. E. Schlesinger (1999), The dependence on convection parameterization of the tropical intraseasonal oscillation simulated by the UIUC 11-Layer Atmospheric GCM, *J. Clim.*, *12*(5), 1423–1457, doi:10.1175/1520-0442(1999)012 <1423:TDOCPO>2.0.CO;2.

Wehner, M. F., et al. (2014), The effect of horizontal resolution on simulation quality in the Community Atmospheric Model, CAM5.1, *J. Adv. Model. Earth Syst.*, *6*, 980–997, doi:10.1002/2013MS000276.

Wilks, D. S. (2006), *Statistical Methods in the Atmospheric Sciences*, 2nd ed., edited by R. Dmowska, D. Hartmann, and H. T. Rossby, Academic, Burlington, Mass.

Xie, S. (2004), Impact of a revised convective triggering mechanism on Community Atmosphere Model, Version 2, simulations: Results from short-range weather forecasts, *J. Geophys. Res.*, *109*, D14102, doi:10.1029/2004JD004692.

Yang, S., Z. Zhang, V. E. Kousky, R. W. Higgins, S.-H. Yoo, J. Liang, and Y. Fan (2008), Simulations and Seasonal Prediction of the Asian Summer Monsoon in the NCEP Climate Forecast System, *J. Clim.*, *21*(15), 3755–3775, doi:10.1175/2008JCLI1961.1.

Zadra, A., R. McTaggart-Cowan, P. A. Vaillancourt, M. Roch, S. Bélair, and A.-M. Leduc (2014), Evaluation of tropical cyclones in the Canadian global modeling system: Sensitivity to moist process parameterization, *Mon. Weather Rev.*, *142*(3), 1197–1220, doi:10.1175/MWR-D-13-00124.1.

Zhang, G. J., and M. Mu (2005), Simulation of the Madden–Julian Oscillation in the NCAR CCM3 Using a Revised Zhang–McFarlane Convection Parameterization Scheme, *J. Clim.*, *18*(19), 4046–4064, doi:10.1175/JCLI3508.1.

Zhang, J. A., and F. D. Marks (2015), Effects of horizontal diffusion on tropical cyclone intensity change and structure in idealized three-dimensional numerical simulations, *Mon. Weather Rev.*, *143*(10), 3981–3995, doi:10.1175/MWR-D-14-00341.1.

Zhang, Y., and S. A. Klein (2010), Mechanisms affecting the transition from shallow to deep convection over land: Inferences from observations of the diurnal cycle collected at the arm southern great plains site, *J. Atmos. Sci.*, *67*(9), 2943–2959, doi:10.1175/2010JAS3366.1.